Tidal ellipses in the near-shore zone (-3 to -10 m); modelling and observations

Klaas T. Houwman[1] and Piet Hoekstra[1]

Abstract

Based on theoretical considerations it is demonstrated that in the near-shore zone the tidal water level fluctuations are mainly caused by cross-shore volume fluxes. Phase differences between the tidal wave propagating on the shelf and in the shallow near-shore zone create cross-shore surface gradients which result in an onshore directed flow during rising water and an offshore directed flow during falling water. Observations of near bed velocities in the near-shore zone confirm the presence of these currents. It results in an anti clockwise rotating current vector at a water depth of about 10m . Comparisons of these observations with results obtained from a 1-DV flow model show that the tidal ellipses are not the result of Coriolis forces but are generated by the alternating cross-shore water fluxes due to the tide.

Introduction

Generally, in the near-shore zone several mechanism are present which are capable of driving a mean flow, e.g. waves, wind and tides. In literature many studies are focussing on wave driven currents, but hardly any study can be found describing the tidal phenomena in the near-shore zone. In this study we will focus on tidal flow phenomena which can be found in the near-shore zone of the barrier island of Terschelling, the Netherlands. Houwman and Uittenbogaard (1998) investigated the longshore tidal flow at this location by combining modelling and observations. Here emphasis will be given to the tide induced cross-shore flow. Measurements as well as model results will be used to investigate the origin of these currents.

Description of the field site and measurements

---

[1] Institute for Marine and Atmospheric Research, Utrecht University, Department of Physical Geography, P.O.Box 80.115, 3508 TC Utrecht, The Netherlands.

For the analysis presented in this paper, data will be used obtained from measurements made in the multiple bar system of the barrier island of Terschelling, the Netherlands. These measurements were carried out in the framework of the NOURTEC project (Hoekstra et al., 1994). The field site is fully exposed to the North Sea, with an average annual offshore significant wave height of 1.1m. Tides are semi diurnal with a neap tidal range of about 1.5 m and a spring tidal range of ca. 2.5 m. The tidal wave propagates along the coast from the west to the east with an almost constant speed and shape within several tens of km's at either side of the measurement site. In a cross-shore direction, the inner near shore zone is characterized by several breaker bars parallel to the shoreline (see figure 1).

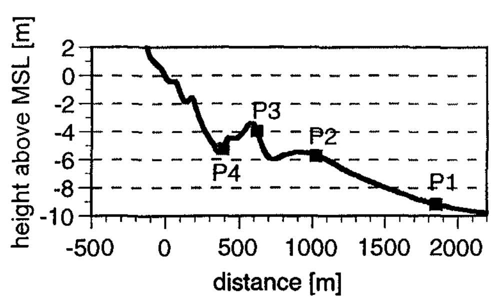

Figure 1: Cross-shore profile with instrumented positions.

The bars are more or less uniform in longshore direction in the area of interest. Several instrumented tripods were placed in a cross-shore transect at position P1, P2, P3 and P4 (see Figure 1) and data was collected over a time period of 2 years during three successive campaigns. All tripods were equipped with two Electro Magnetic Flow meters (EMF) at (nominal) heights of 0.3 m and 1.2 m above the bed and a pressure sensor at 2.2 m above the bed. Each tripod collected data with a sampling frequency of 2 Hz with a burst length of 2048 s and starting at every full hour. These bursts were split up in four subseries of 512 s each and averaged values of these subseries were used for the analyses presented here. Furthermore, from this data set two calm weather events, with a length of about 140 hours each, were selected. The wave height during these periods was in the range of 0.3-0.8 m and wave breaking occurred only landwards of P4. The wind speed during both periods was about 6 m/s.

Flow model

In this study, a one dimensional vertical flow model (1-DV) will be used to support the analysis of measurements. Here the outline of this model will be described briefly. More details, and an evaluation of this model are presented in Houwman and Uittenbogaard (1998). This 1-DV flow model, describes the distribution of the horizontal velocity vector over depth at a single location in the horizontal plane. The equations of motion in cross-shore x and longshore y direction at a particular height z above the bottom are respectively given by:

$$\frac{\partial U}{\partial t} = -g\frac{\partial \zeta}{\partial x} + fV + \frac{\partial}{\partial z}\left(\upsilon_T \frac{\partial U}{\partial z}\right) \tag{1}$$

$$\frac{\partial V}{\partial t} = -g\frac{\partial \zeta}{\partial y} - fU + \frac{\partial}{\partial z}\left(\upsilon_T \frac{\partial V}{\partial z}\right) \tag{2}$$

In this U and V are the orthogonal velocity components in x and y direction respectively. The first left-hand terms describe the rate of change of the velocities. The horizontal pressure gradient is represented by the first right-hand term, with ζ being the water level fluctuation around mean sea level. The Coriolis force is given by the second right-hand term, with the Coriolis parameter f=2ΩsinΦ representing the influence of the earth's rotation. The last right-hand term describes the vertical exchange of horizontal momentum due to the turbulent forces. The eddy viscosity υ_T is calculated from the Kolmogorov-Prandtl expression, using a standard k-ϵ turbulence model. The equations of this turbulence model, with their constant settings, are adopted from Launder and Spalding (1974). Assuming a logarithmic velocity profile in the near-bed region and in the region near the air-water interface leads to the boundary conditions for this k-ϵ turbulence model.
The boundary conditions for the flow equations (1) and (2) can be deduced making the same assumption. The bottom boundary condition for eq.(1) reads:

$$\upsilon_T \frac{\partial U}{\partial z}\bigg|_{z=z_0} = S^2 U\sqrt{U^2+V^2} \tag{3}$$

The parameter S is given by $S = \kappa / \ln(z/z_0)$, with the Von Kármán' constant κ and roughness length z_0. Similar conditions are used at the upper boundary and for eq. (2). The cross-shore water surface gradient $\partial\zeta/\partial x$ is obtained from a method given by Uittenbogaard and Van Kester (1996). They used the depth-integrated version of the equation of motion to calculate the surface gradient. Here this method is applied to calculate the cross-shore surface gradient $\partial\zeta/\partial x$:

$$g\frac{\partial \zeta}{\partial x}\bigg|_t = \frac{\tau_{sx} - \tau_{bx}}{\rho h} + \frac{\overline{U}(t-T_{rlx}) - \overline{U_0}}{T_{rlx}} + f\overline{V} \tag{4}$$

with :
- τ_{sx} = surface shear stress in cross-shore direction
- τ_{bx} = bottom shear stress in cross-shore direction
- h = water depth
- T_{rlx} = some relaxation time span
- $\overline{U}(t-T_{rlx})$ = depth averaged cross-shore velocity solution at time t - Δt

$\overline{U_0}$ = given depth averaged cross-shore velocity at time t

$\overline{V}$ = depth averaged longshore velocity solved

The cross-shore surface gradient can be calculated from eq. (4) using information about the shear stresses at the boundaries and the depth averaged currents. The shear stress τ_{bx} and the depth averaged currents $\overline{U}(t\text{-}T_{rlx})$ and $\overline{V}$ are obtained from the solution of eq. (1) and (2) while the surface stress component τ_{sx} is an input term of the model (wind stress). The depth averaged velocity $\overline{U_0}$ must be specified and is an input parameter for the model. Using alternatingly eq.(1), (2) and (4), the depth averaged velocity $\overline{U}$ at time t - T_{rlx} approaches the velocity $\overline{U_0}$. The surface gradient then balances the shear stresses at the surface τ_{sx} and the bottom τ_{bx} and the (small) contribution of the Coriolis force. The time step T_{rlx} is taken equal to two times the numerical time step which results in a stable and accurate solution.
The prescribed depth averaged (cross-shore) velocity $\overline{U_0}$ is set to zero for the entire tidal cycle. Note that this does not mean that the cross-shore velocity at each position in the vertical is zero. Finally, specification of the longshore surface gradient $\partial\zeta/\partial y$ and the roughness length z_0 is needed, to apply the model. Here the longshore surface gradient, obtained from measured water levels at two locations along the coast, is used to drive the model. A fixed roughness length z_0 of 0.0033 m was used for all computations, based on the findings of Houwman and Van Rijn (1998) for the same site. All computations were carried out, using 100 grid points equally distributed over the vertical, and 16 time steps in an hour. The model is capable to reproduce the observed longshore velocities accurately as shown by Houwman and Uittenbogaard (1998).

Results

The model was run for the first selected period of 140 hours at position P1 and the calculated flow pattern at 1.2 m above the bed is shown in figure 2. The calculated current ellipse is almost flat and is orientated parallel to the coast. Note that the horizontal and vertical axises are different in this diagram. In principle the combination of the Coriolis force and the cross-shore pressure gradient should produce a clockwise rotating current vector at the surface and an anticlockwise sense of rotation for the current ellipse at the bottom. But at this water depth of about 10 m, the vertical gradient of the Coriolis forcing term is rather small. The depth averaged contribution of the Coriolis force in cross-shore direction $f\overline{V}$ is balanced by the cross-shore water surface gradient. So, the difference between the Coriolis force $f\,V$ and the depth averaged Coriolis force $f\overline{V}$ is the only net driving force left for the cross-shore flow. The combination of this small driving force and a strong friction in the vertical results in an almost rectilinear flow pattern. Figure 2 also presents the measured flow pattern for the same period and location. In contrast to the predicted flow pattern, the observations show a clear developed ellipse. This ellipse is apparently not caused by Coriolis forces because these were taken into account in the model. The difference between predicted and observed cross-shore velocities can be explained in the following way: In the model the depth averaged cross-shore flow is taken equal to zero. Using this condition one assumes implicitly that at each location the volume of water involved in the rising or falling of the water level is fully delivered by the longshore tidal flow. This can easily be seen from the continuity equation (5). Taking $\overline{U}=0$ implies that the first term is balanced by the third term .

$$\frac{\partial\zeta}{\partial t}+\frac{\partial h\overline{U}}{\partial x}+\frac{\partial h\overline{V}}{\partial y}=0 \tag{5}$$

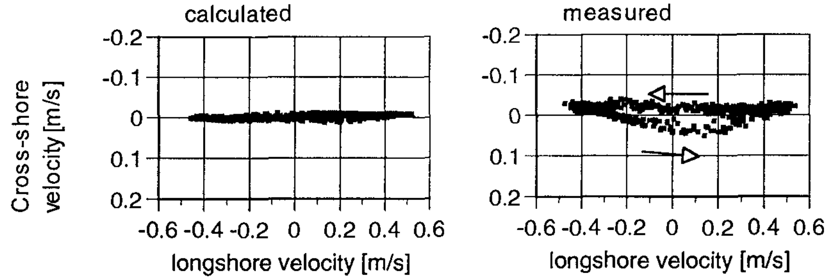

Figure 2: Calculated and measured flow pattern at P1, 1.2 m above the bed.

A scale analysis however, shows that this is not the case in thc near-shore zone. Assuming a tidal wave with amplitude ζ_1 , period T ,wavelength L and depth averaged longshore velocity $\overline{V}_1$, the first and last term in the continuity equation have the following order of magnitude:

$$\begin{aligned}&\frac{\partial\zeta}{\partial t}\approx O\left(\frac{\zeta_1}{T}\right)\\&\frac{\partial\overline{V}h}{\partial y}=h\frac{\partial\overline{V}}{\partial y}+\overline{V}\frac{\partial h}{\partial y}\approx O\left(d\frac{\overline{V}_1}{L}+\overline{V}_1\frac{\zeta_1}{L}\right)\end{aligned} \tag{6}$$

The magnitude of these terms becomes comparable at a mean water depth d $\approx$24m, when typical values for the tidal regime at Terschelling are used. At smaller water depths $\partial\zeta/\partial t$ is significant larger than the $\partial\overline{V}h/\partial y$ term. So, at these water depths a cross-shore flux must be present. The actual magnitude of the $\partial\zeta/\partial t$ and $\partial\overline{V}h/\partial y$ terms can more accurately be deduced using the flow model. The magnitude of the $\partial\overline{V}h/\partial y$ term can be calculated assuming a longshore uniform topography and using the propagation speed of the tidal wave. These computations demonstrate that the term $\partial\overline{V}h/\partial y$ is significant smaller than the $\partial\zeta/\partial t$ term at a mean water depth of 10 m. Averaged over a half tidal cycle, about 22% of the volume of water is delivered by this longshore term at this water depth. At smaller water depths the importance of the $\partial\overline{V}h/\partial y$ term decreases rapidly. For example, at a water depth of 5 m approximately 6% of the volume flux is delivered by the longshore term and at 2 m water depth only 1% can be explained from this. This implies that in the near shore zone the second term in the continuity equation $\partial\overline{U}h/\partial x$, is nonzero and is mainly responsible for delivering the volume of water associated with the tidal water level fluctuations in the coastal zone. The relative importance of this cross-shore term grows for a decreasing water depth. The underlying reason for this cross-shore flux is the difference in water depth on the shelf and in the near-shore zone. The tidal wave propagates along the coast with a speed determined by the (average) water depth at the shelf. In the shallow near-shore zone the propagation speed would have been less as a result of the smaller water depth, which is of course not possible. The tide in the near-shore zone lags the propagation of the tidal wave at the shelf only slightly. But, this results in co-tidal lines which are not entirely perpendicular to the coast. This is schematically illustrated in figure 3.

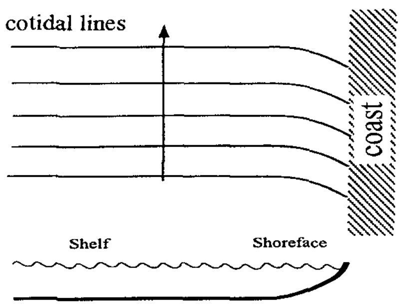

Figure 3: Cotidal lines on the shelf and shoreface.

During rising water the water level in deep water rises faster than in the shallow near shore zone. This results in a cross-shore water surface gradient which drives an onshore directed, cross-shore flow (see figure 4). This flow is (mainly) responsible for increasing the water level in the shallow near-shore zone. During falling water the reversed process will take place and an offshore directed flow will be present, as indicated in figure 4.

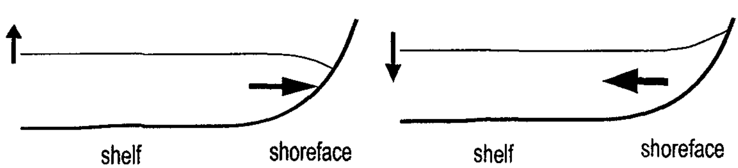

Figure 4: Cross-shore flow due to tide induced surface gradients.

So, in colour full terms spoken, the tidal wave in the near-shore zone is drawn along the coast by the tidal wave travelling on the shelf. The principle of this tide induced cross-shore flow is also described by Pugh (1987). Unfortunately, the magnitude of this cross-shore flow can not be deduced from a 1-DV model, at least a 2-DH model is required. But in the near-shore zone the third term in the continuity equation is relatively small as shown above. Therefore a reasonable approximation of the magnitude of the cross-shore flow can be found after neglecting this longshore term in the continuity equation. After integration in cross-shore direction from a position x_0 to the waterline, see figure 5, the following expression is found:

$$\overline{U_0} = \frac{x_0}{h}\frac{\partial \zeta}{\partial t} \tag{7}$$

So, the depth averaged flow at a particular position in the near shore-zone depends on the distance to the waterline x_0 , the local water depth h and the rate of fluctuation of the water level. The flow $\overline{U_0}$ delivers a water volume to the landwards located zone, equal to the dotted area presented in figure 5.

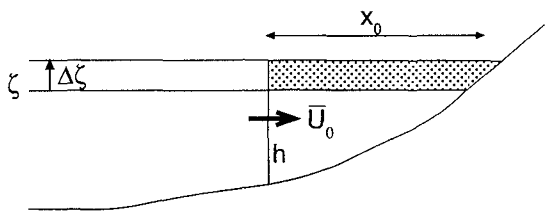

Figure 5: The tide induced cross-shore flow in the near-shore zone.

The distance to the water line x_0 depends on the actual water level and is thus a function of time. It can be calculated from: $x_0 = x_1 + \zeta/\tan\beta$. In this x_1 is the distance to the waterline when $z = 0$ (mean sea level) and $\tan\beta$ is the slope of the beach, which is 0.014 m/m in the Terschelling case. Figure 6 shows the computed cross-shore distribution of the depth averaged cross-shore flow during one tidal cycle. During falling water (time 0 to 5) an offshore (negative) flow is present at all positions and during rising water (time 6 to 11) an onshore (positive) flow exists at each position. Due to the asymmetry of the water elevation curve, the onshore directed currents are larger than the offshore directed ones, but the duration of this latter period is longer. The largest velocities are found just after low tide. At that time the most rapid variation of the water level takes place. The cross-shore distribution of the tidal flow clearly shows a relationship with the morphology. The largest velocities can be found on top of the bars and local minima in the spatial flow distribution coincide with the troughs. Further offshore also rather strong velocities are predicted. But, one has to keep in mind that at water depths larger then ~8 m the contribution of the longshore term in the continuity equation becomes significant resulting in a reduction of $\overline{U_0}$. The magnitude of the cross-shore flow depends on the speed in which the water level is changing. The largest flow velocities coincide with the steepest parts of the tidal elevation curve. For these periods the longshore surface slope is also maximal. Without inertia, this would result in maximum cross-shore and longshore flow at the same time, creating a rectilinear flow pattern oblique to the coast. The influence of the inertia is however significant for the longshore flow, which results in a phase lag between cross-shore and longshore flow. Therefore an anticlockwise rotating current vector can be expected at locations where inertia plays a significant role, see figure 2. In contrast to velocity profiles affected by Coriolis forces this mechanism creates a current vector which rotates in the same direction at every position in the vertical. The direction of rotation has of course nothing to do with Coriolis forces, it is determined by

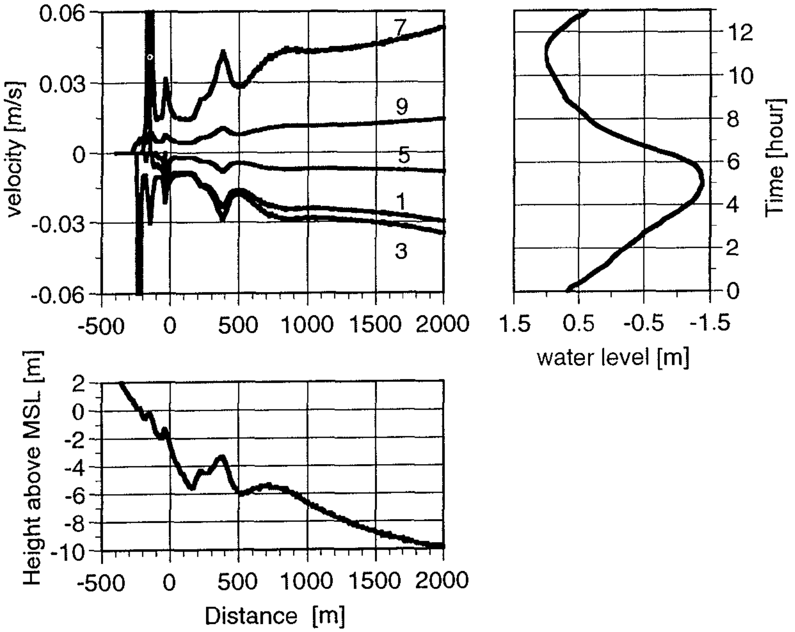

Figure 6: Cross-shore distribution of the tide induced depth averaged cross-shore flow.

the position of the coast, left or right relative to the progressive tidal wave.

This mechanism, generation of a tide induced cross-shore flow, can easily be implemented into the flow model simply using eq. (7) to calculate the model input parameter $\overline{U_0}$ for every time step.

Computations were carried out, using this condition, for the two selected periods of 140 hours each. Figure 7 shows the observed and calculated tidal ellipses during the first period at P1 at 1.2 m and 0.3 m above the bed. The computed as well as the observed flow patterns show ellipses created by an anticlockwise rotating current vector. The predictions agree well with the observations. The tide induced cross-shore velocities at these levels are rather small, with a typical maximum value of about 0.05 m/s at 1.2 m above the bed. Figure 8 shows the flow pattern at P1 during the second period of 140 hours. The computed velocities during this period form an anticlockwise rotating current vector similar to the previous period. The measured velocities however do not show a clear ellipsoidal form. Unfortunately, the orientation of the measured flow pattern is not accurately known due to inaccuracies in the determination of the direction of the flow meter in the frame. So, it is not clear if the phase lag between long and cross-shore flow has become less or that the cross-shore flow is diminished during this period. It is also

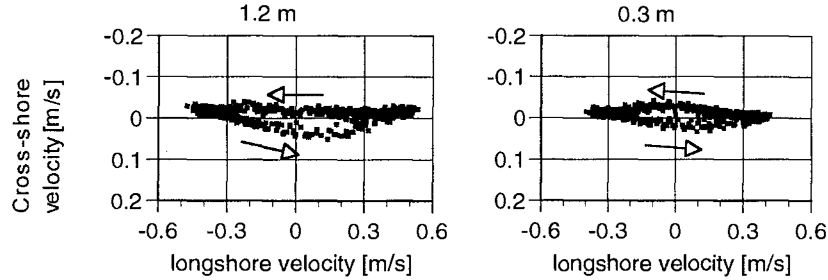

Figure 7a: Measured flow pattern at P1 during the first period

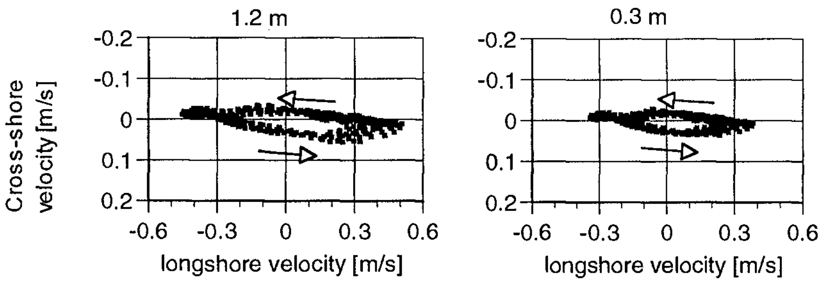

Figure 7b: Predicted flow pattern at P1 during the first period.

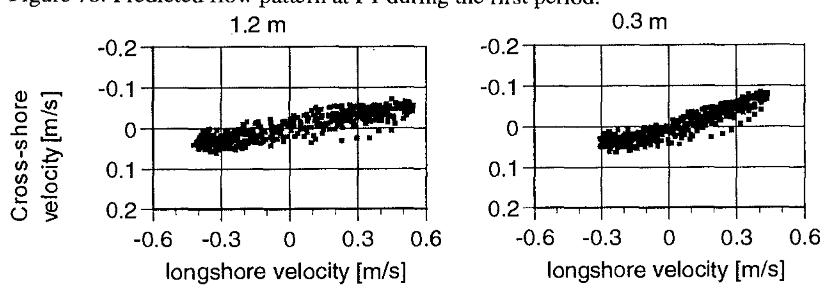

Figure 8a: Measured flow pattern at P1 during the second period.

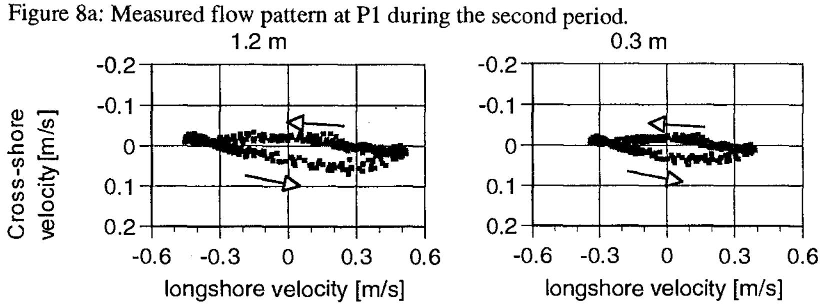

Figure 8b: Predicted flow pattern at P1 during the second period.

unclear why in the second period the observed ellipses are flat, contrary to the ones in the first period, but at station P2 the same phenomena occurred. During the second period the observed velocities at P2 do not form an ellipse in contrast to the predicted ones .The ellipses observed during the first period are shown in figure 9 together with the calculated ones.

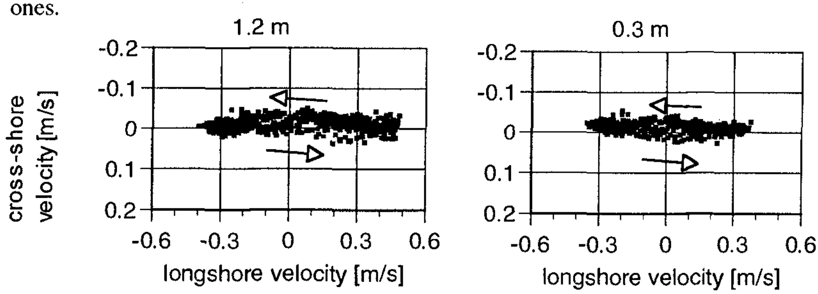

Figure 9a: Measured flow pattern at P2 during the first period.

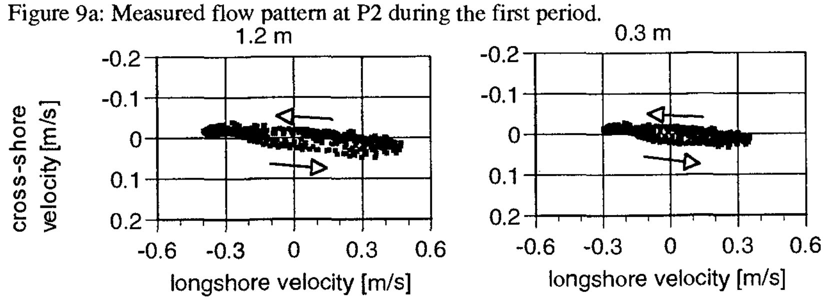

Figure 9b: Predicted flow pattern at P2 during the first period.

Although the observed ellipses are less "open" as the computed ones, they both display similar trends. The onshore velocities are larger than the offshore directed velocities, which is also visible in figure 7 and 8. The shape of the predicted tidal ellipses at P1 and P2 is different, which is the result of a decrease of the phase lag between the longshore and cross-shore flow. The influence of the inertia on the flow at P2 is smaller than at P1 resulting in a reduction of this phase lag. The measured and predicted tidal ellipses during the second period at this position P2 are shown in figure 10. At position P3 and P4 only data from the second period is available. The measured and computed ellipses at station P3 for this period are shown in figure 11. Also here the current vectors predicted by the model rotate in an anticlockwise sense. And again, onshore directed current velocities are larger than the offshore directed ones. At this position with a mean water depth of about 4 m the influence of the inertia on the flow is small, which results in an almost flat ellipse. The main axis of this ellipse makes an angle with the coast line. The predictions and observations do not deviate significantly from each other, taking into account the error band in the orientation of the flow meter.

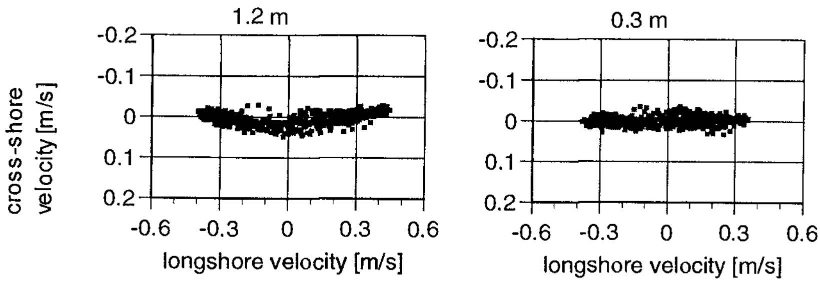

Figure 10a: Measured flow pattern at P2 during the second period.

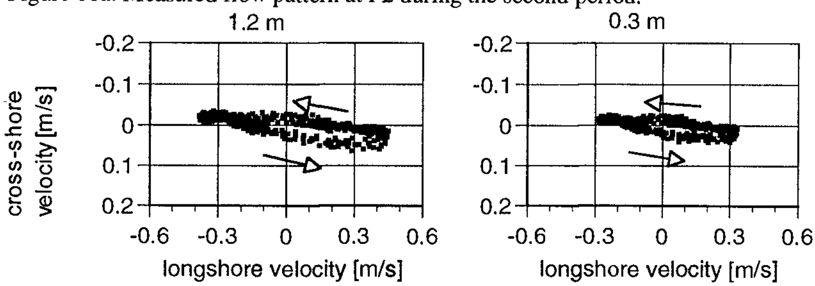

Figure 10b: Predicted flow pattern at P2 during the second period.

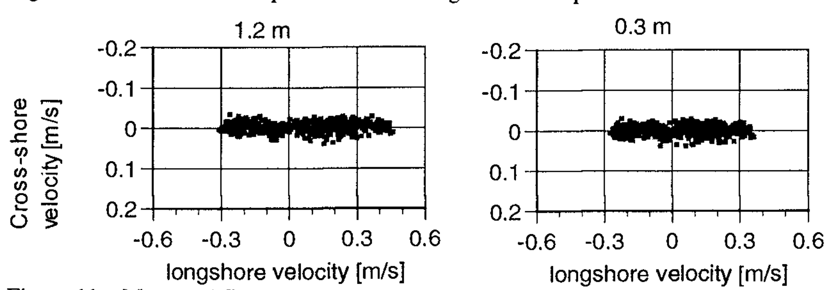

Figure 11a: Measured flow pattern at P3 during the second period.

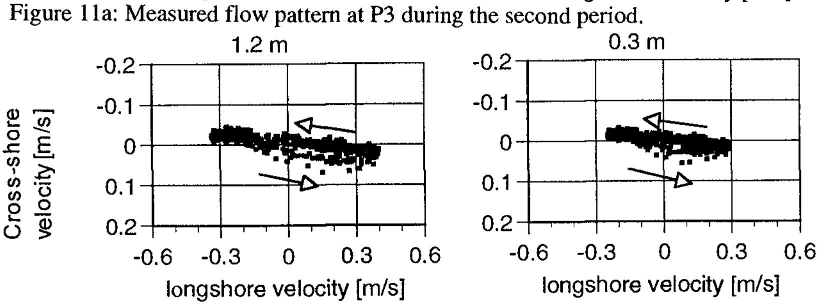

Figure 11b: Predicted flow pattern at P3 during the second period.

Figure 12 shows the measured and predicted current ellipses in the trough at station P4. The observations and the model results indicate that no clear ellipses are developed at this position. This can be explained by the combination of a relative large water depth at this position and the rather small distance to the shore. The measured velocities are somewhat scattered and the flood current at 0.3 m above the bed seems to be deflected. The reason for this is not clear.

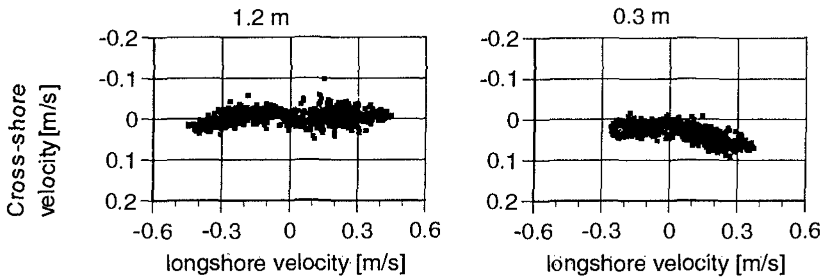

Figure 12a: Measured flow pattern at P4 during the second period.

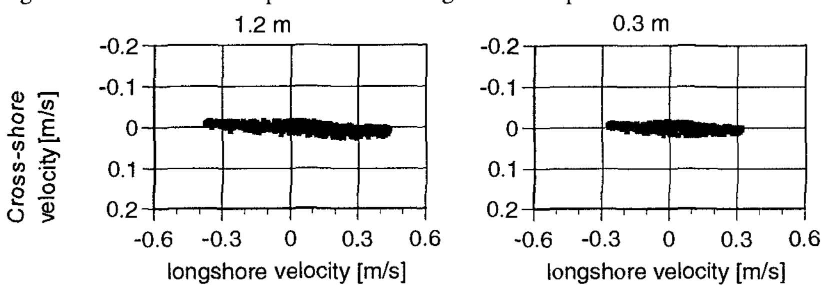

Figure 12b: Predicted flow pattern at P4 during the second period.

Discussion and conclusions

Based on theoretical considerations it is demonstrated that small but persistent cross-shore flows are generated in the near-shore zone due to tidal water level fluctuations. This is confirmed by the comparison between model computations and flow observations. A phase difference between the tidal wave in the near-shore zone and on the shelf creates cross-shore surface gradients which drives a cross-shore flow. At this site the volume flux involved in the tidal fluctuation of the water level in the near-shore zone, at water depths less than 10 m, is mainly delivered by the cross-shore flow. Neglecting the contribution of the longshore flow to this volume flux makes it possible to determine this cross-shore flow. The magnitude of the tide induced cross-shore flow depends on the tidal range, the shape of the tidal curve, the local water depth, the distance to the water line and the slope of the beach. Furthermore, the propagation speed of the tidal wave is important, if one takes the longshore term, the third term in eq. (5), into account.

Based on this, it can be expected that this mechanism is important only for coastal areas dealing with a meso or macro tide and a gentle sloping beach-shoreface system such as the coast of Terschelling.

The comparison of observed and predicted tidal ellipses demonstrates that the tide induced cross-shore currents can be detected in the field. Predictions of the near bed flow at a water depth of about 10m (location P1) indicate that ellipses can be expected, which were also observed in the field during the first period. But, in contrast to the predictions, no clear ellipse was observed during the second period. A similar result was found at P2. Apparently, the flow pattern can easily be disturbed by other mechanisms. Non-uniformity of the morphology in longshore direction could be an explanation for the difference between measured and predicted ellipses during the second period. But, particular at position P1, the large scale morphology is uniform over several kilometres in longshore direction and is almost identical for both periods. So, it is unlikely that this is the reason for the observed differences. Perhaps wind effects play a role in this, although no significant differences were present during the first and second period. A decrease of the phase differences between longshore and cross-shore velocities, which are small, could explain the diminishing of the open ellipses. A time shift, for any reason whatsoever, in the order of 20 minutes would already give a flat ellipse which makes an angle to the coastline. These flat ellipses have been observed, but the magnitude of the cross-shore flow in those cases can not be determined due to the inaccuracies in the direction of the measured flow vector. At this stage, it remains unclear what the reason is for the disturbance of the ellipse. It is clear though persistent, tide induced cross-shore currents exist. Going from P1 further inshore, the phase difference between longshore and cross-shore near bed flow decreases, resulting in a change of the shape of the tidal ellipse. At P3, the major axis of predicted ellipses is oblique orientated to the coast and the minor axis is only small compared to the one at P1 .

Finally, at P4 a rectilinear flow pattern is predicted, orientated shore parallel, which is the result of the rather large water depth and the short distance to the shore line.

Acknowledgments

This work was carried out in the framework of the NOURTEC project: Innovative Nourishment Techniques Evaluation. It was jointly funded by the Ministry of Transport, Public Works and Water Management in the Netherlands and by the Commission of the European Communities, Directorate General for Science, Research and Development under the Marine Science and Technology programme: MAS2-CT93-0049.

References

Hoekstra, P., Houwman, K.T., Kroon, A., Vessem, P. Van and Ruessink, B.G., 1994:The NOURTEC experiment of Terschelling: process-oriented monitoring of a shoreface nourishment (1993-1996). Proc. Coastal Dynamics'94, ASCE, 402-416.

Houwman, K.T. and Uittenbogaard, R.E., 1998:The vertical distribution of the flow field in the near-shore zone: a comparison between model results and measured tidal velocities. Submitted to Journal of Physical Oceanography, AMS.

Houwman, K.T. and Van Rijn, L.C., 1998: Modelling the apparent bed roughness under varying wave and current conditions in the field. Submitted to Coastal Engineering, Elsevier.

Launder, B.E. and Spalding, D.B., 1974: The numerical computation of turbulent flows. Computer methods in applied mechanics and engineering, 3, 269-289.

Pugh, D.T., 1987: Tides, surges and mean sea-level. John Wiley & Sons, 472 pp.

Uittenbogaard, R.E. and Van Kester, J.A.Th.M., 1996: Modelling seasonal temperature stratification with TRIWAQ. A preparatory study based on one-dimensional computations, Report Z978, Delft Hydraulics, The Netherlands, 89 pp.